Journal of Power Sources 196 (2011) 4152–4161

Contents lists available at ScienceDirect

Journal of Power Sources

journal homepage: www.elsevier.com/locate/jpowsour

Low band gap dyes based on 2-styryl-5-phenylazo-pyrrole: Synthesis and application for efficient dye-sensitized solar cells

J.A. Mikroyannidis[a,*], D.V. Tsagkournos[a], P. Balraju[b,c], G.D. Sharma[b,d,**]

[a] Chemical Technology Laboratory, Department of Chemistry, University of Patras, Rion, GR-26500 Patras, Greece
[b] Physics Department, Molecular Electronic and Optoelectronic Device Laboratory, JNV University, Jodhpur (Raj.) 342005, India
[c] Molecular Electronics Laboratory, JNCASR, Bangalore, India
[d] R&D Center for Science and Engineering, Jaipur Engineering College, Kukas, Jaipur (Raj.), India

ARTICLE INFO

Article history:
Received 22 October 2010
Received in revised form
30 November 2010
Accepted 11 December 2010
Available online 21 December 2010

Keywords:
Pyrrole
Azo dyes
Low band gap
Dye-sensitized solar cells
Electron lifetime

ABSTRACT

A new series of low band gap dyes, **C1**, **C2** and **S**, based on 2-styryl-5-phenylazo-pyrrole was synthesized. These dyes contain one carboxy, two carboxy and one sulfonic acid anchoring groups, respectively. They were soluble in common organic solvents, showed long-wavelength absorption maximum at ~620 nm and optical band gap of 1.66–1.68 eV. The photophysical and electrochemical properties of these dyes were investigated and found to be suitable as photosensitizers for dye sensitized solar cells (DSSCs). The quasi solid state DSSCs with dye **S** showed a maximum monochromatic incident photon to current efficiency (IPCE) of 78% and an overall power conversion efficiency (PCE) of 4.17% under illumination intensity of 100 mW cm^{-2} (1.5 AM), which is higher than the other dyes (3.26% for **C2** and 2.59% for **C1**). Even though dye **S** contains one sulfonic acid anchoring group, the higher PCE for the DSSCs based on this dye has been attributed to the higher dye loading at the TiO_2 surface and enhanced electron lifetime in the device, as indicated by absorption spectra and electrochemical impedance spectra measurements. Finally, by increasing the molecular weight of poly(ethylene oxide) (PEO) in electrolyte, the PCE also increases up to 4.8% for the electrolyte with PEO molecular weight of 2.0×10^6. This improvement has been attributed to the enhancement in iodide ions diffusion due to the increase in free volume of polymer gel electrolyte.

1. Introduction

Due to the advantages of low cost, easy production, flexibility, and transparency relative to conventional crystalline silicon solar cells, dye-sensitized solar cells (DSSCs) have emerged as an important class of photovoltaic (PV) devices, since the breakthrough was made by Grätzel and co-workers [1]. Significant progress was made in terms of the performance of DSSC devices. In particular, power conversion efficiencies (PCEs) above 11% in standard global air mass (AM) 1.5 have been achieved by several Ru^{II}–polypyridyl complexes [2], while 6–9% was shown by metal-free organic dyes [3]. Although the efficiency of the latter was slightly lower, they possessed some advantages over the former: ease of synthesis, high molar extinction coefficient, tunable absorption spectral response from the visible to the near infrared (NIR) region, as well as environmentally friendly and inexpensive production techniques. Furthermore, the solid state DSSCs based on metal free dyes show higher PV performance than those based on Ru dyes, due to the higher molar absorption coefficients (attributed to intramolecular π–π^* transition) of these dyes [4]. To further improve the efficiencies of pure organic dye-based DSSCs, the structure and physical properties of the sensitizer are clearly important, especially the conjugation across the donor and anchoring groups, and good electronic coupling between the lowest unoccupied orbital (LUMO) of the dye and the conduction band of TiO_2, which is very important for high electron-transfer rates [5]. Consequently, in order to exploit such sensitizers, it is necessary to lower the energy of the charge-transfer transition. In this respect, some electron-rich heteroaromatic rings have been used as bridges between electron donor and acceptor. Specifically, some thiophene and furan containing dyes exhibited good device efficiencies [6], due to their smaller resonance energy in comparison with that of benzene. However, the analogue of furan and thiophene moieties, that is pyrrole group, has seldom been used as a conjugated bridge in organic dyes [7], possibly due to its unstability, although it possesses a smaller resonance energy, and could be easily funtionalized, not

* Corresponding author. Tel.: +30 2610 997115; fax: +30 2610 997118.
** Corresponding author at: Physics Department, Molecular Electronic and Optoelectronic Device Laboratory, JNV University, Jodhpur (Raj.) 342005, India. Tel.: +91 0291 2720857; fax: +91 0291 2720856.
E-mail addresses: mikroyan@chemistry.upatras.gr, mikroyan@googlemail.com (J.A. Mikroyannidis), sharmagd_in@yahoo.com (G.D. Sharma).

0378-7753/$ – see front matter © 2010 Elsevier B.V. All rights reserved.
doi:10.1016/j.jpowsour.2010.12.038

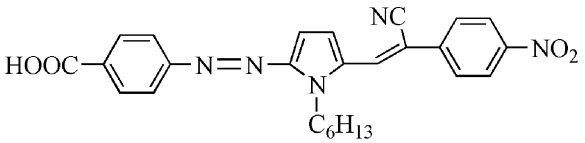

C1

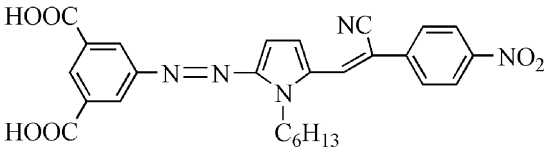

C2

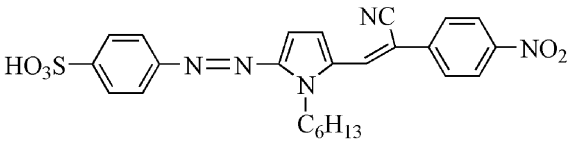

S

Scheme 1. Chemical structures of dyes **C1**, **C2** and **S**.

only on the ortho-position to the nitrogen atom, but also through the substituted reactions on the N–H bond [8].

On the other hand, the synthesis and properties of azo dye based polymers and materials has drawn a considerable amount of attention due to their applications as reversible optical storage media, chiroptical switches, electrooptic modulators, and chemical sensors [9,10]. Over the past decade, there has been a number of articles and patents detailing the use of azo dyes as sensors [11,12]. Azo dyes combine their optical and electronic properties with good chemical stability and solution processability [13,14], which makes them interesting for applications. Nevertheless, there is a small number of reports on DSSCs with azo dyes as sensitizers.

Recently, we have synthesized three new bisazopyrrole dyes and the corresponding BF_2–azopyrrole complexes. These symmetrical dyes contain carboxy or hydroxy anchoring groups at both sides of their molecules. We have utilized these complexes as photosensitizers for DSSCs and achieved PCE in the range of 4.0–6.0% [15]. Moreover, we have synthesized three new organic sensitizers with carboxy, acid anhydride or hydroxy anchoring groups and terminal cyanovinylene 4-nitrophenyl segments and used them for DSSCs [16]. The maximum PCE of 4.58% has been obtained from the sensitizer with carboxy anchoring group which has been further improved up to 5.80%, by adding chenodeoxyacholic acid coadsorbent in the dye solution [16].

The present investigation describes the synthesis of three new dyes **C1**, **C2** and **S** based on 2-styryl-5-phenylazo-pyrrole (Scheme 1). Dyes **C1** and **C2** contain one and two carboxy anchoring groups, respectively, while dye **S** contains one sulfonic acid anchoring group. 1-Hexylpyrrole is the central unit of these dyes which is connected with substituted-phenylazo at one side and with cyanovinylene 4-nitrophenyl at the other side of the pyrrole ring. Both these terminal moieties extended the absorption band of the dyes into the near infrared region, which is a desirable feature for PV applications. In addition, the hexyl chain attached to the nitrogen of pyrrole enhanced the solubility of the dyes. These dyes were successfully synthesized by a four-step reaction sequence and combine the properties of the azo compounds with those of cyanovinylene 4-nitrophenyl. These dyes contain various anchoring groups which are expected to affect the PV properties of DSSCs. They were investigated as photosensitizers in DSSCs, using polymer gel quasi solid state electrolyte as redox mediator. The overall PCE for these devices are 4.17, 3.26 and 2.59% for **S**, **C2** and **C1** respectively. The higher PCE for the DSSCs based on **S** has been attributed to the enhanced dye loading at the TiO_2 surface and improved electron lifetime, which retards the recombination of the injected electrons with iodide ions present in the electrolyte. Finally, we have investigated the influence of the molecular weight of the PEO on the performance of quasi solid state DSSC based on dye **S** and achieved PCE of 4.8% for the PEO molecular weight of 2.0×10^6. The improvement in the PCE is mainly attributable to the increase in the short circuit current (J_{sc}), which is related to the enhancement in iodide ion diffusion due to the increase in fee volume of polymer gel electrolyte.

2. Experimental

2.1. Reagents and solvents

4-Nitrobenzylcyanide was synthesized from the nitration of benzyl cyanide with concentrated nitric and sulfuric acid [17]. It was recrystallized from ethanol. 4-Aminobenzoic acid and 5-aminoisophthalic acid were recrystallized from distilled water. *N*,*N*-Dimethylformamide (DMF) and tetrahydrofuran (THF) were dried by distillation over CaH_2. All other reagents and solvents were commercially purchased and were used as supplied.

2.2. Synthesis of dyes and precursor compounds

2.2.1. 1-Hexyl-1H-pyrrole (**1**)

A flask was charged with a mixture of pyrrole (1.00 g, 14.9 mmol), 1-bromohexane (2.46 g, 14.9 mmol), THF (15 mL), NaOH (0.70 g, 17.5 mmol) and 18-Crown-6 (10 mg) as phase transfer catalyst (PTC). The mixture was stirred and refluxed for 15 h under N_2. Then, it was concentrated under reduced pressure. Water (20 mL) was added to the concentrate and it was extracted twice with dichloromethane (2×15 mL). The organic layer was dried (Na_2SO_4) and concentrated to yield **1** as a brownish oil. It was purified by distillation under reduced pressure (0.94 g, 42%). The spectroscopic characterization of **1** conforms to literature [18].

2.2.2. 1-Hexyl-1H-pyrrole-2-carbaldehyde (**2**)

A flask was charged with DMF (0.67 g, 9.22 mmol). Phosphorus oxychloride (1.41 g, 9.22 mmol) was added dropwise at 0 °C to DMF. The cooling bath was removed and stirring was continued for 15 min. The solution was diluted with 1,2-dichloroethane (20 mL) and again cooled to 0 °C. A solution of **1** (1.27 g, 8.38 mmol) in 1,2-dichloroethane (10 mL) was added dropwise. The mixture was heated to reflux for 15 min. Sodium acetate (3.78 g, 46.08 mmol) dissolved in water (25 mL) was added at 0 °C to the mixture with vigorous stirring. The mixture was refluxed for 20 min and then cooled at room temperature. The aqueous layer was separated and extracted twice with dichloromethane. The combined organic layers were washed with $NaHCO_3$ solution until neutral, dried (Na_2SO_4) and concentrated to yield **2**. It was purified by column chromatography (ethyl acetate:hexane 1:9) to afford **2** (1.23 g, 82%). The spectroscopic characterization of **2** conforms to literature [19].

2.3. Compounds *4a*, *4b* and *4c*

2.3.1. 4-((5-Formyl-1-hexyl-1H-pyrrol-2-yl)diazenyl)benzoic acid (*4a*)

The preparation of **4a** is given as a typical example: a flask was charged with a suspension of 4-aminobenzoic acid (0.4485 g, in

water 8 mL). Hydrochloric acid (2 mL) was added to the suspension. The mixture was cooled and kept at 0–5 °C in an ice bath and diazotized by adding a solution of $NaNO_2$ (0.2500 g, 3.60 mmol) in water (5 mL) followed by stirring for 0.5 h at 0–5 °C. The solution of the diazonium salt (**3a**) thus prepared was immediately used for the next coupling reaction.

The solution of **3a** was slowly added to a solution of **2** (0.5863 g, 3.27 mmol) and pyridine (3 mL) in ethanol (30 mL) at 0–5 °C. The resulting mixture was stirred for 10 h and then concentrated under reduced pressure. The precipitate was filtered, washed with dilute hydrochloric acid, then with water and dried to afford **4a**. It was purified by column chromatography (dichloromethane:hexane 1:1). Yield 87% (0.93 g).

FT-IR (KBr, cm^{-1}): 3200 (O–H stretching of carboxyl); 2954, 2926, 2856 (C–H stretching of hexylene); 1712 (C=O stretching of carboxyl); 1694 (formyl).

^1H NMR ($CDCl_3$) ppm: 9.80–9.50 (br, 2H, carboxyl and formyl); 8.12 (m, 2H, phenylene ortho to carboxyl); 7.43 (m, 2H, phenylene meta to carboxyl); 7.01 (m, 1H, H3 of pyrrole); 6.34 (m, 1H, H4 of pyrrole); 4.31 (t, J = 7.1 Hz, 2H, NCH_2); 1.73 (m, 2H, NCH_2CH_2); 1.27 (m, 6H, $N(CH_2)_2(CH_2)_3$); 0.86 (t, J = 6.8 Hz, 3H, $N(CH_2)_5CH_3$).

Anal. Calcd. for $C_{18}H_{21}N_3O_3$: C, 66.04; H, 6.47; N, 12.84. Found: C, 65.84; H, 6.32; N, 12.96.

2.3.2. 5-((5-Formyl-1-hexyl-1H-pyrrol-2-yl)diazenyl)isophthalic acid (**4b**)

FT-IR (KBr, cm^{-1}): 3392 (O–H stretching of carboxyl); 2954, 2928, 2856 (C–H stretching of hexylene); 1714 (C=O stretching of carboxyl); 1708 (formyl).

^1H NMR ($CDCl_3$) ppm: 9.90–9.40 (br, 3H, carboxyl and formyl); 8.53–8.23 (m, 3H, phenylene ortho to carboxyl); 7.00 (m, 1H, H3 of pyrrole); 6.33 (m, 1H, H4 of pyrrole); 4.30 (t, J = 7.1 Hz, 2H, NCH_2); 1.74 (m, 2H, NCH_2CH_2); 1.28 (m, 6H, $N(CH_2)_2(CH_2)_3$); 0.86 (t, J = 6.8 Hz, 3H, $N(CH_2)_5CH_3$).

Anal. Calcd. for $C_{19}H_{21}N_3O_5$: C, 61.45; H, 5.70; N, 11.31. Found: C, 61.37; H, 5.85; N, 11.12.

2.3.3. 4-((5-Formyl-1-hexyl-1H-pyrrol-2-yl)diazenyl)benzenesulfonic acid (**4c**)

FT-IR (KBr, cm^{-1}): 3460–3180 (sulfonic acid); 2954, 2926, 2856 (C–H stretching of hexylene); 1704 (formyl).

^1H NMR ($CDCl_3$) ppm: 9.53–9.34 (br, 2H, sulfonic acid and formyl); 8.21 (m, 2H, phenylene ortho to sulfonic acid); 7.50 (m, 2H, phenylene meta to sulfonic acid); 7.02 (m, 1H, H3 of pyrrole); 6.32 (m, 1H, H4 of pyrrole); 4.31 (t, J = 7.1 Hz, 2H, NCH_2); 1.73 (m, 2H, NCH_2CH_2); 1.28 (m, 6H, $N(CH_2)_2(CH_2)_3$); 0.88 (t, J = 6.7 Hz, 3H, $N(CH_2)_5CH_3$).

Anal. Calcd. for $C_{17}H_{21}N_3O_4S$: C, 56.18; H, 5.82; N, 11.56. Found: C, 56.03; H, 5.69; N, 11.36.

2.4. Dyes **C1**, **C2** and **S**

2.4.1. (Z)-4-((5-(2-Cyano-2-(4-nitrophenyl)vinyl)-1-hexyl-1H-pyrrol-2-yl)diazenyl)benzoic acid (**C1**)

The preparation of **C1** is given as a typical example: a flask was charged with a solution of **4a** (0.9303 g, 2.84 mmol) and 4-nitrobenzylcyanide (0.4608 g, 2.84 mmol) in ethanol (20 mL). Sodium hydroxide (0.20 g, 5.00 mmol) dissolved in ethanol (10 mL) was added to this solution. The reaction mixture was stirred for 1 h at room temperature under N_2 and then it was concentrated under reduced pressure. Water (20 mL) and then hydrochloric acid (2 mL) were added to the concentrate and **C1** precipitated as a dark green solid. It was recrystallized from ethanol/water (1.14 g, 86%).

FT-IR (KBr, cm^{-1}): 3182 (O–H stretching of carboxyl); 2954, 2926, 2856 (C–H stretching of hexylene); 2198 (cyano); 1715 (C=O stretching of carboxyl); 1524, 1342 (nitro).

^1H NMR ($CDCl_3$) ppm: 9.53 (s, 1H, carboxyl); 8.24–8.10 (m, 4H, phenylene ortho to carboxyl and nitro); 7.80 (s, 1H, vinylene); 7.60–7.44 (m, 4H, phenylene meta to carboxyl and nitro); 6.22 (m, 2H, pyrrole); 4.30 (t, J = 7.1 Hz, 2H, NCH_2); 1.75 (m, 2H, NCH_2CH_2); 1.28 (m, 6H, $N(CH_2)_2(CH_2)_3$); 0.87 (t, J = 6.7 Hz, 3H, $N(CH_2)_5CH_3$).

Anal. Calcd. for $C_{26}H_{25}N_5O_4$: C, 66.23; H, 5.34; N, 14.85. Found: C, 66.04; H, 5.28; N, 14.96.

2.4.2. (Z)-5-((5-(2-Cyano-2-(4-nitrophenyl)vinyl)-1-hexyl-1H-pyrrol-2-yl)diazenyl)isophthalic acid (**C2**)

FT-IR (KBr, cm^{-1}): 3400 (O–H stretching of carboxyl); 2954, 2924, 2856 (C–H stretching of hexylene); 2208 (cyano); 1710 (C=O stretching of carboxyl); 1528, 1344 (nitro).

^1H NMR ($CDCl_3$) ppm: 9.50 (s, 2H, carboxyl); 8.54–8.18 (m, 5H, phenylene ortho to carboxyl and nitro); 7.80 (s, 1H, vinylene); 7.50 (m, 2H, phenylene meta to nitro); 6.22 (m, 2H, pyrrole); 4.32 (t, J = 7.1 Hz, 2H, NCH_2); 1.73 (m, 2H, NCH_2CH_2); 1.27 (m, 6H, $N(CH_2)_2(CH_2)_3$); 0.86 (t, J = 6.7 Hz, 3H, $N(CH_2)_5CH_3$).

Anal. Calcd. for $C_{27}H_{25}N_5O_6$: C, 62.91; H, 4.89; N, 13.59. Found: C, 62.53; H, 5.03; N, 13.45.

2.4.3. (Z)-4-((5-(2-Cyano-2-(4-nitrophenyl)vinyl)-1-hexyl-1H-pyrrol-2-yl)diazenyl)benzenesulfonic acid (**S**)

FT-IR (KBr, cm^{-1}): 3470–3190 (sulfonic acid); 2954, 2928, 2856 (C–H stretching of hexylene); 2210 (cyano); 1526, 1346 (nitro).

^1H NMR ($CDCl_3$) ppm: 9.38 (br, 1H, sulfonic acid); 8.20–8.10 (m, 4H, phenylene ortho to sulfonic acid and nitro; 7.81 (s, 1H, vinylene); 7.60–7.40 (m, 4H, phenylene meta to sulfonic acid and nitro); 6.21 (m, 2H, pyrrole); 4.29 (t, J = 7.2 Hz, 2H, NCH_2); 1.74 (m, 2H, NCH_2CH_2); 1.29 (m, 6H, $N(CH_2)_2(CH_2)_3$); 0.87 (t, J = 6.8 Hz, 3H, $N(CH_2)_5CH_3$).

Anal. Calcd. for $C_{25}H_{25}N_5O_5S$: C, 59.16; H, 4.96; N, 13.80. Found: C, 59.04; H, 5.17; N, 13.92.

2.5. Characterization methods

IR spectra were recorded on a Perkin-Elmer 16PC FT-IR spectrometer with KBr pellets. ^1H NMR (400 MHz) spectra were obtained using a Brucker spectrometer. Chemical shifts (δ values) are given in parts per million with tetramethylsilane as an internal standard. UV–vis spectra were recorded on a Beckman DU-640 spectrometer with spectrograde THF. Elemental analyses were carried out with a Carlo Erba model EA1108 analyzer.

Cyclic voltammetry (CV) measurements of the materials were performed with an Autolab analyzer using three electrodes electrochemical cell in a solution of tetra butylammonium hexafluorophosphate (Bu_4NPF_6) (0.1 M) in anhydrous acetonitrile at a scan rate of 100 mV s^{-1} at room temperature. Dye deposited on TiO_2 coated FTO conducting glass was used as the working electrode, a Pt wire as the counter electrode and an Ag/Ag^+ electrode as reference electrode.

2.6. Fabrication of quasi solid state DSSCs and characterization

TiO_2 paste was prepared by mixing 1 g of TiO_2 powder (P25, Degussa) 0.2 mL of acetic acid and 1 mL of water. Then, 60 mL of ethanol was slowly added while sonicating the mixture for 3 h. Finally, Triton X-100 was added to obtain a dispersed colloidal (TiO_2) paste. The mixture was stirred vigorously for 2–4 h at room temperature and then stirred for 4 h at 80 °C to form a transparent

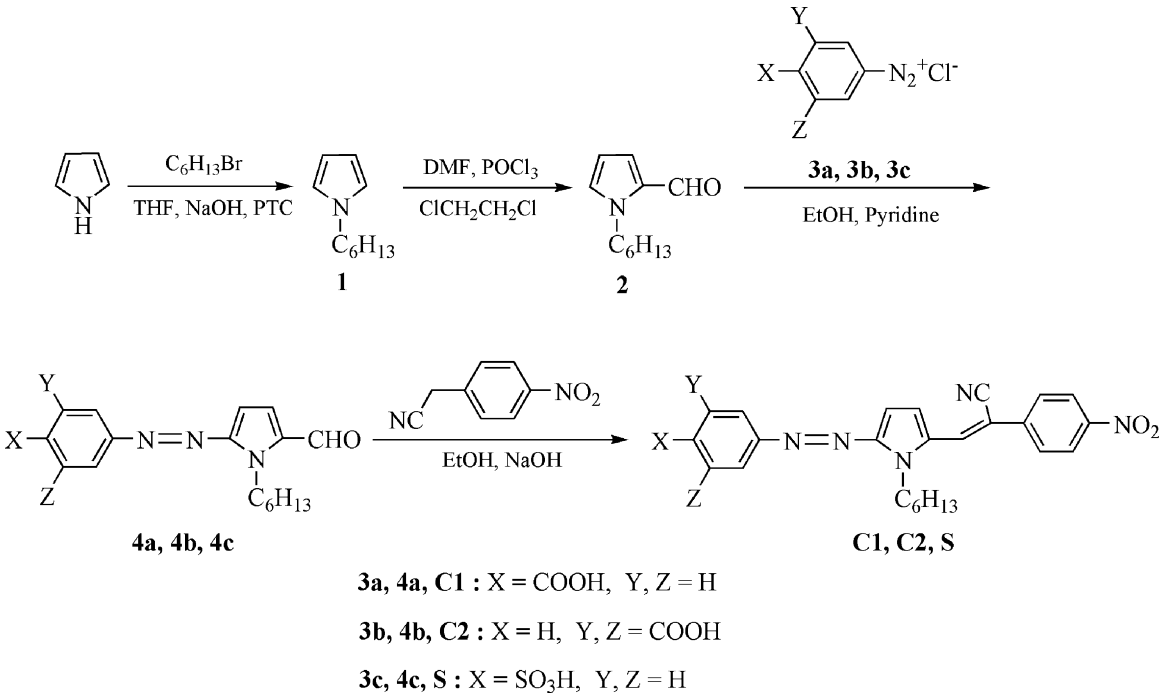

Scheme 2. Synthesis of dyes **C1**, **C2** and **S**.

colloidal (TiO_2) paste. The TiO_2 paste was deposited on the precleaned fluorine (F) doped tin oxide (FTO) coated glass substrate by the doctor blade technique. The TiO_2 coated FTO films were sintered at 450 °C for 30 min and cooled down up to room temperature. Before immersing into the dye solution, these films were soaked in a 0.2 M aqueous $TiCl_4$ solution overnight in a closed chamber. After being washed with deionized water and fully rinsed with ethanol, the films were again sintered at 450 °C for 30 min, followed by cooling up to 60 °C.

The dyes were dissolved in acetonitrile solution (0.5 mM) and the TiO_2 coated electrode (area 0.26 cm^2) was immersed in the dye solution overnight. After sensitization, the electrode was washed and then dried. A quasi solid state polymer gel electrolyte containing 0.0383 g of P25 TiO_2 powder, 0.1 g of LiI, 0.019 g of I_2, 0.264 g of poly(ethylene oxide) (PEO) and 44 μL of 4-*tert*-butylpyridine (TBP) in 1:1 acetonitrile/propylene carbonate was prepared. The mixture was continuously stirred at 80 °C in a water bath for about 4–5 h. The polymer gel electrolyte was spread on the sensitized TiO_2 film by spin coating to form the hole transport layer. The counter electrode was platinized by spin coating H_2PtCl_6 solution (2 mg in 1 mL of isopropanol) onto the FTO coated glass substrate and then heated at 450 °C for 30 min in air. The dye sensitized photoelectrode containing the quasi solid state polymer electrolyte and the counter electrode were clamped together and separated by 15 μm.

The current–voltage (*J*–*V*) characteristics of the devices in dark and under illumination were measured by a semiconductor parameter analyzer (Keithley 4200-SCS). A xenon lamp light source (Oriel, USA) was used to give an irradiance of 100 mW cm^{-2}) (the equivalent of one sun at 1.5 AM) at the surface of the device. The incident photon to current conversion efficiency (IPCE) spectra of the devices were measured using a monochromator (Spex 500 M, USA) and the resulted photocurrent was measured with Keithley electrometer (model 6514), which is interfaced to the computer by LABVIEW software. The value of the accumulated extracted charge (Q_{sc}) was determined by the following measurement. The solar cell was biased at the voltage equivalent of the open circuit voltage of the corresponding device in dark for 5 s, and the current was measured under short circuit conditions in <20 s, and then the current was integrated to obtain Q_{sc} [20].

The electrochemical impedance spectra (EIS) measurements were carried out by applying bias of the open circuit voltage (V_{oc}) and recorded over a frequency range of the 1 mHz to 10^5 Hz with an amplitude of 10 mV. The above measurements were recorded with an electrochemical analyzer equipped with FRA.

3. Results and discussion

3.1. Synthesis and characterization

Scheme 2 outlines the four-step reaction sequence for the synthesis of the target dyes **C1**, **C2** and **S**. In particular, pyrrole reacted with 1-bromohexane in THF in the presence of sodium hydroxide to afford **1**. The latter was formylated by DMF and phosphorus oxychloride to yield **2**. The diazonium salts **3a**, **3b** and **3c** were prepared by reacting 4-aminobenzoic acid, 5-aminoisophthalic acid or 4-aminobenzenesulfonic acid, respectively, with $NaNO_2$/aqueous HCl at temperature 0–5 °C. These diazonium salts reacted immediately after their preparation with one equivalent of **2** in ethanol neutralized with pyridine to give the corresponding azo-compounds **4a**, **4b** and **4c**. Finally, they were condensed with 4-nitrobenzylcyanide in ethanol in the presence of sodium hydroxide to afford the sodium salts of **C1**, **C2** and **S** respectively. The free acids were obtained as dark green solids by acidification with hydrochloric acid.

All dyes were soluble in common organic solvents such as THF, dichloromethane and chloroform due to the hexyl chain. Their FT-IR spectra showed characteristic absorption bands around 2210 (cyano); 1525, 1345 (nitro) and 2954, 2925, 2856 (C–H stretching of hexylene). Moreover, **C1** and **C2** displayed absorptions at 3400–3200 (O–H stretching of carboxyl) and 1715 cm^{-1} (C=O stretching of carboxyl). Finally, **S** showed a broad absorption at 3470–3190 cm^{-1} (sulfonic acid). It is well known that the azo groups give weak absorptions which are overlapped with those of the aromatic and therefore they can not be identified by IR

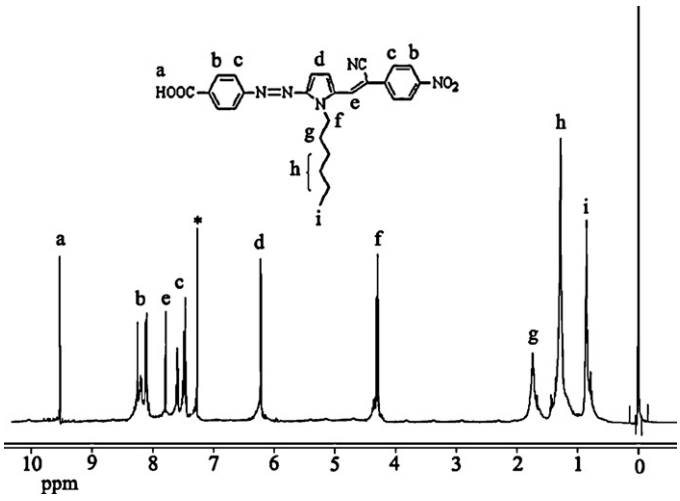

Fig. 1. ^{1}H NMR spectrum of dye **C1** in $CDCl_3$ solution. The peak of the solvent is denoted by an asterisk.

spectroscopy [21]. Fig. 1 presents typical ^{1}H NMR spectrum of **C1**. It showed an upfield signal at 9.53 ppm associated with the carboxyl. The phenylene protons ortho and meta to carboxyl/nitro resonated at 8.24–8.10 and 7.60–7.44 ppm respectively. The signals at 7.80 and 6.22 ppm are assigned to the vinylene and pyrrole respectively. Finally, the hexylene chain resonated at the region of 4.30–0.87 ppm.

3.2. Photophysical properties

Fig. 2 depicts the UV–vis absorption spectra of the dyes in dilute (10^{-5} M) THF solution and thin film. Table 1 summarizes the photophysical and electrochemical properties of the dyes. Their absorption spectra showed short-wavelength peaks at 350–400 nm associated with the n–π^* transitions. Moreover, they displayed a broad long-wavelength absorption maximum ($\lambda_{a,max}$) around 620 nm. The latter was attributed to an intramolecular charge transfer (ICT) between the electron-donating 1-hexylpyrrole and the electron-withdrawing cyanovinylene 4-nitrophenyl. Dye **S** showed more pronounced long-wavelength absorption, especially in thin film, than the other dyes. Generally, the absorption curves of the dyes are similar thus indicating that the different anchoring groups did not influence significantly their absorption. The thin film absorption onset was located at 750 nm for **C1** and **C2** and 741 nm for **S** which corresponds to an optical band gap (E_g^{opt}) of 1.66 and 1.68 eV respectively. These values of E_g^{opt} are in agreement of those of other related materials containing cyanovinylene 4-nitrophenyl segments [16].

Table 1
Optical and electrochemical properties of dyes.

	Dye		
	C1	**C2**	**S**
$\lambda_{a,max}$ [a] in solution (nm)	625	615	602
$\lambda_{a,max}$ [a] in thin film (nm)	625	625	631
Thin film absorption onset (nm)	750	750	741
E_g^{opt} [b] (eV)	1.66	1.66	1.68
HOMO (eV)	−5.0	−5.0	−5.0
LUMO (eV)	−3.26	−3.25	−3.28
E_g^{el} [c] (eV)	1.74	1.75	1.72

[a] $\lambda_{a,max}$: the absorption maxima from the UV–vis spectra in THF solution or in thin film.
[b] E_g^{opt}: optical band gap determined from the absorption onset in thin film.
[c] E_g^{el}: electrochemical band gap determined from cyclic voltammetry.

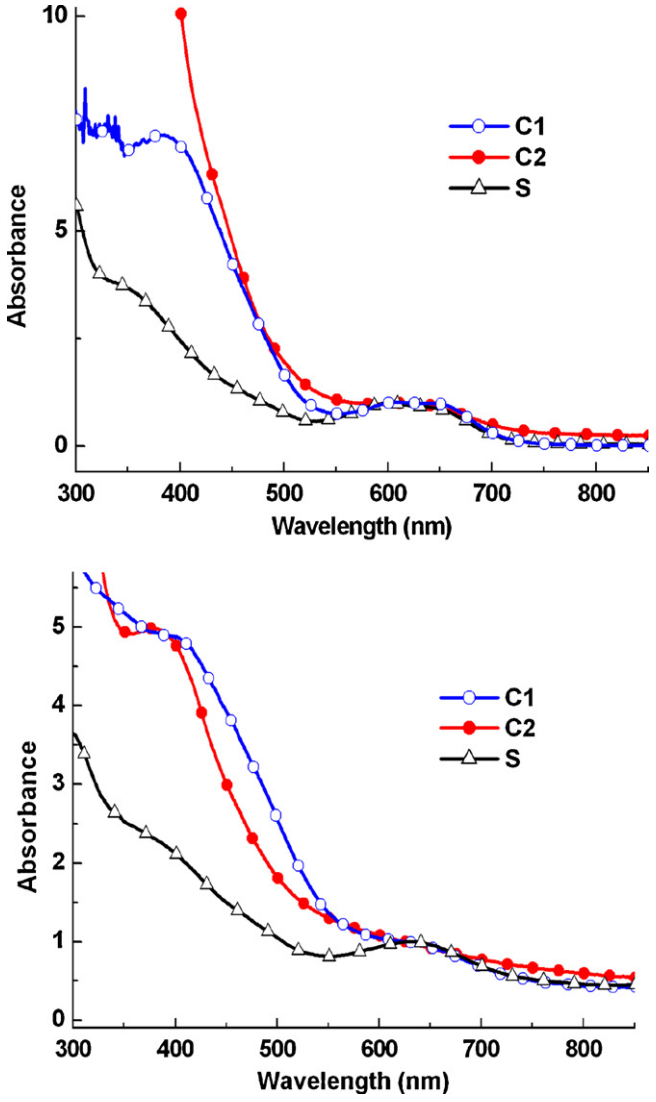

Fig. 2. Normalized UV–vis spectra of dyes in THF solution (top) and thin film (bottom).

3.3. Electrochemical properties

The position of the highest occupied molecular orbital (HOMO) and lowest unoccupied molecular orbital (LUMO) of the organic dyes used as photosensitizer play an important role in the PV performance of the DSSCs. The oxidation potential (E_{ox}) and reduction potential (E_{red}) corresponding to the HOMO and LUMO levels of the dyes were measured by CV. The HOMO and LUMO energy levels of the dyes are estimated from the onset oxidation (E_{ox}) and reduction potential (E_{red}) observed in CV using the following expressions [22]:

$$E_{LUMO} = -q(E_{red} + 4.70)\,eV$$

$$E_{HOMO} = -q(E_{ox} + 4.70)\,eV$$

The unit of the oxidation and reduction potentials are with respect to Ag/Ag^+ potential (4.7 eV vs vacuum). The HOMO and LUMO values are summarized in Table 1. It has been well established that the HOMO and LUMO levels of an organic material are mainly affected by the electron donor and electron acceptor group, respectively. All dyes have common structural features and they are differentiated from the number and the chemical struc-

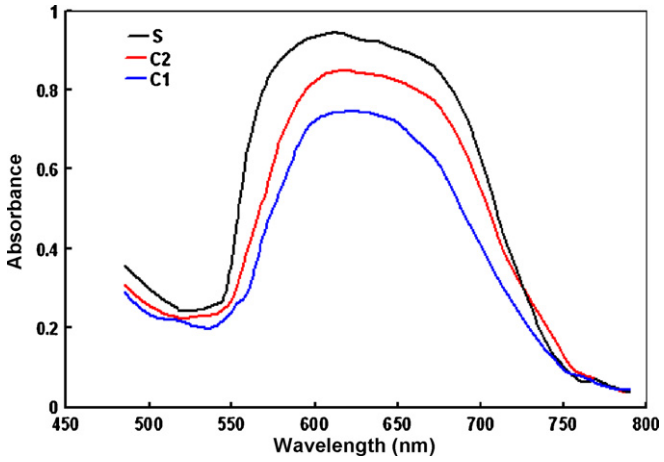

Fig. 3. UV–vis spectra of **S**, **C1** and **C2** dyes adsorbed onto TiO_2 thin films.

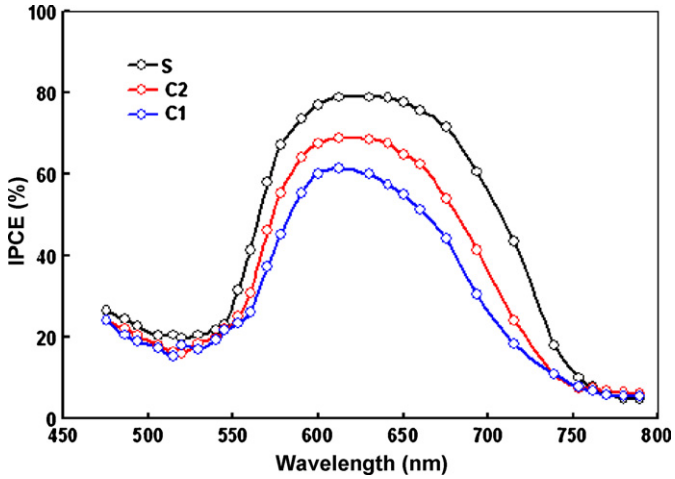

Fig. 4. IPCE spectra of quasi solid state DSSCs based of **S**, **C1** and **C2** dyes.

ture of the anchoring groups (Scheme 1). The HOMO level of all dyes is at the same energy position, but the LUMO level is slightly changed which may be attributed to the different anchoring groups. Thus from the data shown in Table 1 we can conclude that the electron donating ability of these dyes is of the order **S** > **C2** > **C1**. The values of E_{ox} for all dyes are sufficiently more positive than the redox potential of I^-/I_3^- redox mediator (about −4.83 eV vs vacuum) in the electrolyte [23], indicating that the oxidized dye, formed after the electrons injection into the conduction band of TiO_2, could accept electrons from I^- ions in the electrolyte thermodynamically. Moreover, it is evident that the LUMO level for all dyes are more negative than the conduction band edge of TiO_2 (E_{cb} = −4.1 eV vs vacuum) [24]. Consequently, all the dyes can complete the process of electron injection into the conduction band of TiO_2 to form the excited state of oxidized dyes. The energy gap between the excited state (LUMO level) and the conduction band of the TiO_2 is different for all dyes, which indicates that the electron injection efficiency is different of all DSSCs. However, the energy gap between the ground state (HOMO level) and the redox potential of electrolyte is almost the same indicating that the regeneration efficiency of the oxidized dye by I^- is the same for all DSSCs.

3.4. Absorption spectra of dyes adsorbed on TiO_2 films

The absorption spectra of the dyes adsorbed on TiO_2 films are shown in Fig. 3. When the dye is attached to TiO_2 film, the absorption spectra are slightly blue shifted and broadened as compared to those in solution. This broadening is because of strong interactions between the dye and nanocrystalline semiconductor surface. This kind of interactions can also lead to aggregated state of the dye on the nanocrystalline surface which might be correlated with the dye–TiO_2 and dye–dye interactions. The broadening of the absorption spectra of dye adsorbed on TiO_2 film is advantageous for light harvesting efficiency of the DSSCs. By comparing the absorption spectra of dyes adsorbed on TiO_2 films, we observed that the absorption spectrum of **S** sensitized TiO_2 is more broadened relative to **C1** and **C2**. In general, the larger broadening of the dye's absorption spectra on TiO_2 film compared with that in solution shows a tendency to form an aggregation state on TiO_2 film. Suppressing the aggregation of dye on TiO_2 film and anchoring the monolayer of dye into the TiO_2 film are necessary for higher efficiency of DSSCs. The amount of the adsorbed dye on the TiO_2 film was estimated by desorbing the dye with basic solution and the surface concentration was determined to be 6.4×10^{-7}, 3.5×10^{-7} and 2.3×10^{-7} mol cm^{-2} for **S**, **C2** and **C1**, respectively. The dye loading is different for each dye sensitized TiO_2 films; therefore the anchoring group influences the PV performance of the DSSCs, which will be discussed later in the manuscript.

3.5. Photovoltaic properties

The incident photon to current conversion efficiency (IPCE) of the DSSCs was estimated between 400 and 800 nm according to the following expression [24a]:

$$\text{IPCE}\ (\%) = 1240 J_{sc}\ (\text{mA/cm}^2)/\lambda\ (\text{nm})\ P_{in}\ (\text{mW/cm}^2)$$

where J_{sc} is the photocurrent under short circuit condition, λ and P_{in} are wavelength and power of the incident radiation per unit area. Fig. 4 shows the IPCE spectra of DSSCs sensitized by these dyes. The IPCE spectra of all DSSCs resemble the absorption spectra of dyes used for their fabrication. Compared to the DSSCs sensitized by all dyes, the IPCE for the quasi solid state DSSCs sensitized with **S** shows higher value of IPCE than **C1** and **C2**. The IPCE is expressed as [24a]:

$$\text{IPCE}(\lambda) = \text{LHE}(\lambda)\phi_{inj}\eta_c = \text{LHE}(\lambda)\Phi(\lambda)_{ET}$$

where LHE(λ) is the light harvesting efficiency of the photoelectrode, which depends on the amount of dye loading by the electrode and the absorption spectra of the dye adsorbed, ϕ_{inj} is the quantum yield of charge injection from the excited state of dyes into the conduction band of TiO_2, η_c is the efficiency of collecting the injected charge at the back contact and $\Phi(\lambda)_{ET}$ is defined as an electron transfer yield, which is a product of electron injection yield and the charge collection efficiency. Since the absorption spectra and the dye loading by the electrode for all dyes are different, we can assume that the LHE for all the DSSCs is different. We have estimated the dye loading for each DSSC and found the loading is of the order **S** > **C2** > **C1**. The order of the values of IPCE for DSSCs is consistent with the values of dye loading. The absorption spectrum of **S** adsorbed on TiO_2 photoelectrode is more broadened than the other dyes. We assume that the higher LHE may be one of the reasons for the higher value of IPCE for the **S** based DSSC. The charge injection and collection efficiency also affect the IPCE of the DSSCs, which will be discussed later in the manuscript.

The *J–V* characteristics of the DSSCs based on **S**, **C1** and **C2** are shown in Fig. 5 and the PV parameters short circuit current (J_{sc}), open circuit voltage (V_{oc}), fill factor (FF) and power conversion efficiency (PCE) are summarized in Table 2. It can be seen from Table 2 that the PV parameters depend upon the anchoring groups attached to the dyes. The values of both J_{sc} and V_{oc} are higher for the **S** based DSSC.

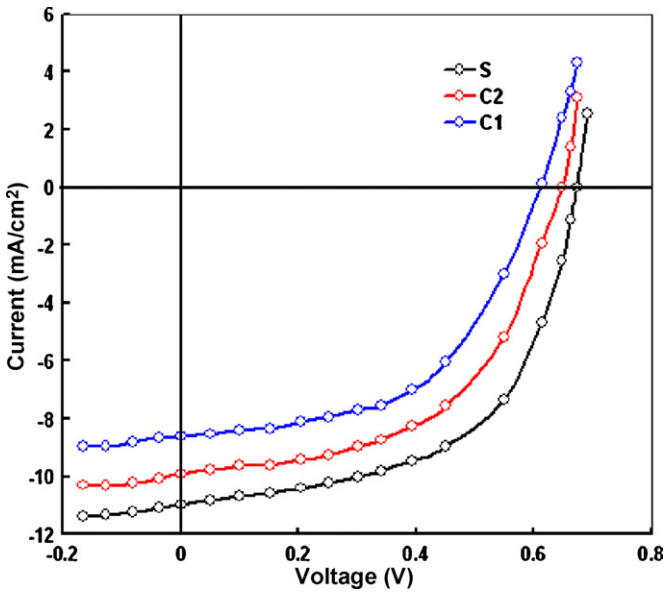

Fig. 5. Photovoltaic performance of DSSCs fabricated from **C1**, **C2** and **S** dyes under stimulated illumination intensity of 100 mW cm^{-2} at AM1.5.

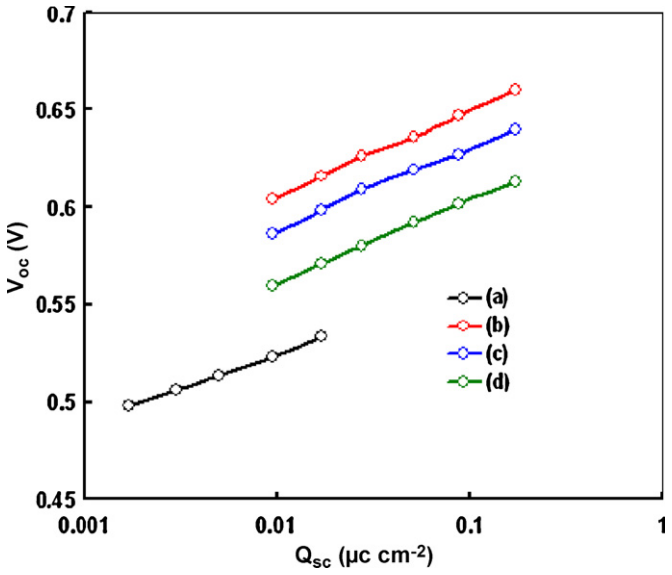

Fig. 6. Dependence of open circuit voltage (V_{oc}) on the extracted charge density (Q_{sc}) for the DSSCs based on (a) bare TiO_2, (b) **S**, (c) **C2** and (d) **C1**.

In principle, the V_{oc} for DSSCs can expressed as [25]:

$$V_{oc} = E_{cb} - \left(\frac{\beta kT}{q}\right) \ln\left(\frac{n}{N_{cb}}\right) - E_{red}$$

where E_{red} is the chemical potential of I^-/I_3^- redox couple, E_{cb} is the conduction band edge of TiO_2, β is a characteristics constant of TiO_2 tailing states, k is the Boltzmann constant, T is the absolute temperature, q is the electronic charge, N_{cb} is the effective density of state at the CB of TiO_2 and n is the electron density in TiO_2. For TiO_2 films prepared under similar conditions, E_{red}, β and N_{cb} do not change strongly. Therefore, the parameters influencing V_{oc} are E_{cb} and n. E_{cb} could be shifted by adsorbed species such as proton, lithium ion and dye molecules, etc. [26].

Since we have used polymer gel electrolyte with the same redox couple for each DSSC, we can assume that the redox potential (E_{red}) for redox couple is constant. The V_{oc} will be determined by the position of the conduction band edge and the concentration of electrons in TiO_2. These two parameters can vary when different dyes are used in the DSSCs. The position of the conduction band edge will be determined by the surface charge supplied by interface species such as ions, additives, and dye molecules. Any change in the surface charge will shift the conduction band edge position and hence the V_{oc}. The number of electrons in TiO_2, n, is determined by the balance between electron injection and electron recombination [27]. We have obtained different values of V_{oc} for DSSCs based on various dyes and this can be attributed to the following reasons: (i) the dyes affect the conduction band edge position of TiO_2 differently, (ii) different dye loading results in different surface blocking, permitting amounts of electron recombination, (iii) the different dye structures yield different electrolyte–dye interactions, hence producing different number of electrolyte acceptors species at the interface, enhancing the electron recombination.

The conduction band (CB) edge position and charge recombination are two essential factors affecting V_{oc}. Under illumination of various light intensities, various values of Q_{sc} have been obtained. At fixed Q_{sc}, an increase in V_{oc} indicates a negative shift in CB, and a decreased V_{oc} indicates a positive shift in CB. Fig. 6 shows the accumulated extracted charge Q_{sc} in DSSCs as a function of V_{oc}. A reference cell based on bare TiO_2 (no dye) was also measured. The CB shift can be determined by plotting V_{oc} against $\ln(Q_{sc})$ derived from the linear fit according to $V_{oc} = V_c + m_c \ln(Q_{sc})$ is calculated as follows.

For bare TiO_2 : $V_{oc} = 630\,\text{mV} + 62\ln(Q_{sc})$

For **S**-TiO_2 : $V_{oc} = 672\,\text{mV} + 61\ln(Q_{sc})$

For $\mathbf{C}_2$-TiO_2 : $V_{oc} = 664\,\text{mV} + 62\ln(Q_{sc})$

For $\mathbf{C}_1$-TiO_2 : $V_{oc} = 658\,\text{mV} + 63\ln(Q_{sc})$

The dye sensitized solar cells showed positive shift up to 42 mV in Q_{sc}–V_{oc} relation compared to the bare TiO_2 case. The shift can be interpreted as shift of the E_{cb} of TiO_2 due to the adsorption of proton released by the anchoring group in the dye, during the dye adsorption. This value is higher for the **S** based DSSC, indicating that more protons are released by **S** thus increasing the dye loading. The more injected electrons in the CB of TiO_2 lead to higher value of V_{oc} for DSSC based on **S** relative to the other dyes [28].

The values of J_{sc} and PCE are also higher for the DSSC based on **S** relative to **C1** and **C2**. Since the value of J_{sc} depends upon the dye loading on the TiO_2 film a recombination rate occurred in the device. As we have discussed earlier, the dye loading is higher for the DSSC based on the **S** than the other dyes indicating that this may be one of reasons for higher J_{sc} and PCE. The more photoinduced charge carriers (as shown in Fig. 6) are generated in the excited state of **S** upon photo-excitation. The order of extracted charge in the DSSCs is **S** > **C2** > **C1** which is also consistent with the values of J_{sc} and PCE. It can be seen that the absorption spectra of **S** adsorbed on TiO_2 and the IPCE spectra of the DSSC based on **S** are more broadened as compared to the other dyes and this could also be attributed to the enhanced J_{sc} and PCE for **S**. Ogomi et al. [29] have demonstrated

Table 2
Photovoltaic parameters, i.e. short circuit current (J_{sc}), open circuit voltage (V_{oc}), fill factor (FF) and power conversion efficiency (PCE) for quasi solid state DSSC based on **S**, **C1** and **C2** dyes.

Dye	J_{sc} (mA cm^{-2})	V_{oc} (V)	FF	PCE (%)
S	10.8	0.69	0.56	4.17
C2	9.6	0.63	0.54	3.26
C1	8.5	0.61	0.50	2.59

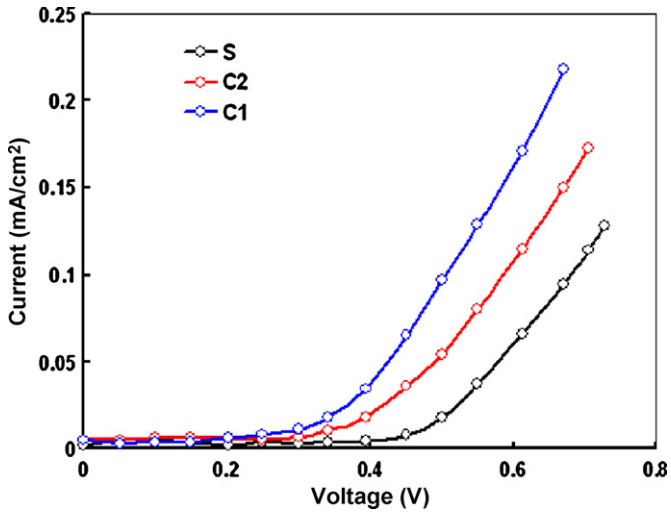

Fig. 7. Dark current–voltage (J–V) characteristics for DSSCs sensitized with **S**, **C1** and **C2** dyes.

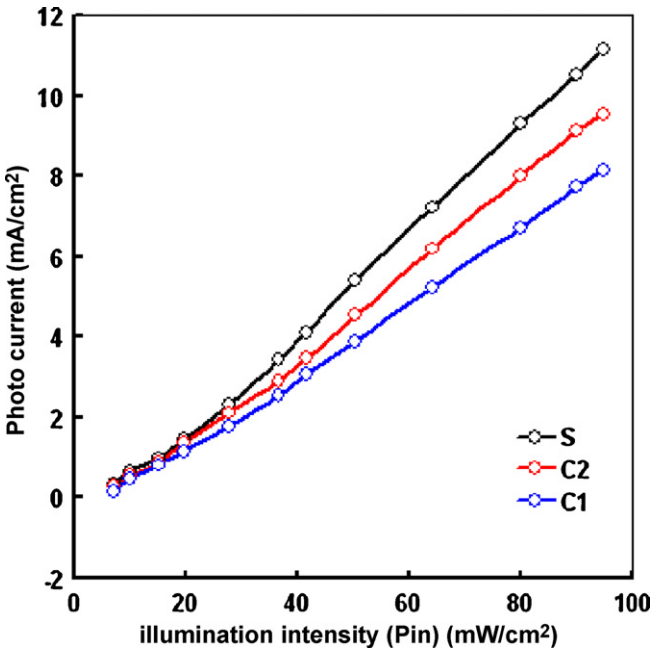

Fig. 8. Variation of photocurrent with illumination intensity for quasi solid state DSSCs based on **S**, **C1** and **C2** dyes.

that increase in the extent of adsorbed dyes on TiO_2 surface leads to enhanced surface traps passivation leading to increased J_{sc}.

The other factor responsible for the enhancement in J_{sc} and PCE is the charge recombination occurring in the device. The charge recombination produces the dark current in the device. The dark J–V characteristics for the DSSCs based on the **S**, **C1** and **C2** are shown in Fig. 7. It can be seen from this figure that the order of dark current onset potential is **S** > **C2** > **C1** and the dark current is minimum for the DSSC based on **S**. This low dark current indicates that the charge recombination between the injected electrons and I_3^- ions in the electrolyte, which is lower for the DSSC based on **S**, favors the enhancement in J_{sc} and PCE. The suppressed charge recombination in DSSCs based on **S** also supports the higher value of J_{sc} and PCE.

Since the amount of the photogenerated electrons is directly proportional to the incident illumination intensity, the variation of J_{sc} with illumination intensity (P_{in}) can be used to obtain information about the amount of photogenerated electrons contributing to the photocurrent and also electron transfer kinetics [30]. Fig. 8 shows that the J_{sc} of the DSSCs for all sensitizers is directly proportional to the P_{in}. This supports that the current density for all DSSCs is limited by both P_{in} and electron transfer. The slope of J_{sc}–P_{in} curve of the DSSCs based on **S**, **C2** and **C1** is about 0.13, 0.10 and 0.092, respectively. The higher value of slope for DSSC based on **S** indicates that more electrons are collected by the FTO electrode. This also indicates that the charge recombination was lower for the DSSC based on **S** as the electron lifetime is longer for this device, thus leading to an increase in the electron collection efficiency.

Electrochemical impedance spectroscopy (EIS) analysis [31] was performed to study the interfacial transfer processes in DSSCs sensitized by different dyes. The Nyquist plots and Bode plots are shown in Fig. 9(a) and (b), respectively. By fitting EIS curves, we can obtain two important parameters for DSSCs. One is the electron lifetime (τ_n), which can be estimated from the frequency (f_p) at the middle frequency peak in the Bode phase plot using $\tau_n = 1/2\pi f_p$ and can be expressed for the electron recombination in TiO_2 films [32]. The other is the electron diffusion length (L_n), which can be expressed for the competition between charge collection and recombination ($L_n = d(R_{ct}/R_t)^{1/2}$, R_{ct} represents charge transfer resistance at dye/TiO_2/electrolyte interface related to the electron recombination, R_t represents the electron transport resistance in TiO_2 film, and d is the thickness of the TiO_2 film) [33]. The electron lifetimes obtained by fitting the Bode plots are 18, 14 and 9 ms for the DSSCs sensitized with **S**, **C2** and **C1**, respectively. The corresponding amount of dye molecules adsorbed on the TiO_2 electrodes were shown to be 6.4×10^{-7}, 3.5×10^{-7} and 2.3×10^{-7} mol cm^{-2}. The electron recombination can be facilitated along with the insufficient coverage on TiO_2 surface, resulting in the decrease in the electron lifetime values [31]. The higher electron lifetime observed for **S** sensitized DSSCs relative to **C1** and **C2** sensitized DSSCs indicates more effective suppression of the back reaction of the injected electron with the I_3^- in the electrolyte,

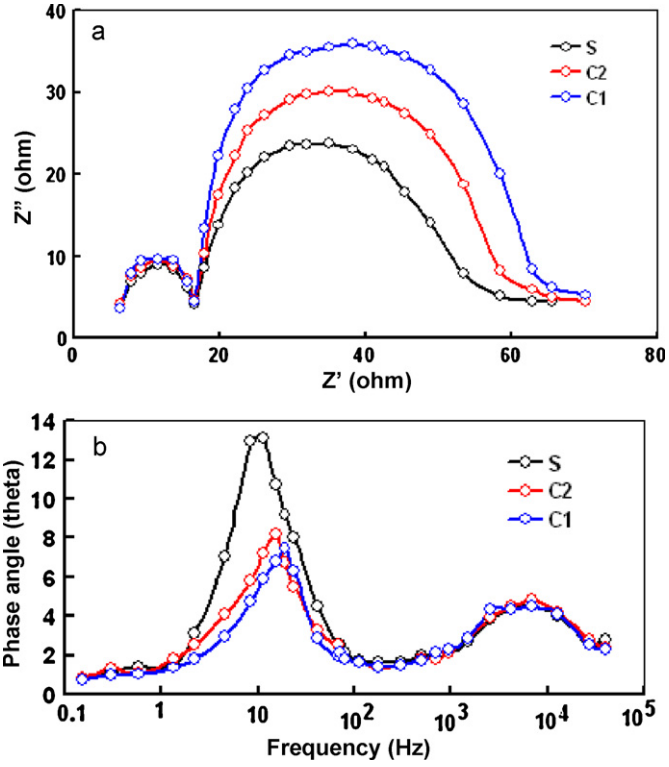

Fig. 9. Electrochemical impedance spectra (EIS) of DSSCs based on **S**, **C1** and **C2**. (a) Nyquist plots and (b) Bode plots.

which is reflected by the improvement seen in the photocurrent yield and the enhanced PCE of the DSSC. The Nyquist plots (Fig. 9a) show the radius of the middle frequency semicircle to decrease in the order **C1** > **C2** > **S**, indicating that the R_t also decreases in the same order. The effective diffusion lengths are 23, 21 and 19 μm for the DSSCs sensitized with **S**, **C2**, and **C1**, respectively. All the effective diffusion lengths are longer than the thickness of the TiO_2 films (18–20 μm), indicating that all photogenerated electrons will be collected efficiently. The higher effective diffusion length and longer electron lifetime for the DSSC sensitized with **S** show that the injected electrons from the excited state of dye into the conduction band of the TiO_2 are more efficiently collected in comparison to **C2** and **C1** sensitized DSSCs. The lowest value of the charge transport resistance (R_t) (315 Ω) for the DSSC based on **S** indicates the higher charge generation and transportation, which corresponds to higher PCE.

3.6. Effect of the molecular weight of PEO on photovoltaic response of DSSC

The PCE of DSSCs based on polymer gel electrolytes is lower than that for liquid electrolytes. Therefore, there has been a great deal of studies on the relationship between the performance of DSSCs and properties of polymer gel electrolytes to improve the energy conversion efficiency of DSSCs based on polymer gel electrolytes. The influencing factors, such as molecular weight of organic solution [34], concentration of alkali metal iodide salts and iodine in the electrolyte [35], kind of gelator [36], and kind of solvent [37] have been investigated. To improve the PCE of the DSSCs based on dye **S** as sensitizer, we have varied the molecular weight of the PEO on the polymer gel electrolyte. We have used PEO of different molecular weight, i.e. $M = 0.5 \times 10^6$, 1.0×10^6, 1.5×10^6 and 2.0×10^6 to prepare the polymer gel electrolyte, while the other components in the polymer gel electrolyte are the same. The ionic conductivities of polymer gel electrolyte at room temperature were measured with conductivity meter which is calibrated with KCl solution (0.1 M) before the experiment. The diffusion behavior of I_3^- in the different polymer gel electrolytes was investigated by measuring the limiting current (I_{lim}) of tri-iodide. The limiting current was determined by linear sweep voltammetry using the device having structure FTO/Pt/polymer gel electrolyte/Pt/FTO. The diffusion coefficient (D) of the ions in polymer gel electrolyte has been obtained according to the following expression [38]:

$$D = \frac{I_{lim} d}{2nFC}$$

where n is the electron per molecule, d is the cell gap, F is the Faraday constant and C is the bulk concentration of electro-active species. It is found that the diffusion coefficient of ions in the polymer gel electrolyte increases with the increase in the molecular weight of PEO.

The J–V characteristics of the DSSCs based on photosensitizer dye **S** with polymer gel electrolyte having different molecular weight of PEO are shown in Fig. 10. The J_{sc} is 10.9, 11.5, 12.2 and 12.9 mA cm^{-2} for DSSC with polymer electrolyte of PEO with molecular weight 0.5×10^6, 1.0×10^6, 1.5×10^6 and 2.0×10^6, respectively. However the V_{oc} is not affected by the variation of molecular weight of PEO. It can be seen that the values of J_{sc} increase notably with increasing the molecular weight of PEO. The overall PCE of the DSSC based on the polymer electrolyte with PEO of molecular weight 2.0×10^6 is 4.8%. We found that the diffusion coefficient of the iodide (I_3^-) ions increases from 2.1×10^{-6} cm^2 s^{-1} ($M = 0.5 \times 10^6$) to 2.8×10^{-6} cm^2 s^{-1} ($M = 2.0 \times 10^6$). The increase in the J_{sc} can be ascribed to the increase of I^- diffusion. The increase in the I_3^- diffusion coefficient is assigned to the enhanced free volume of polymer gel electrolyte with the increase in PEO molecular weight. It is well known that the quasi solid state DSSCs exhibit J_{sc} values lower than that of DSSCs using conventional liquid electrolytes. This is due to the fact that the I^- diffusion is slower in gel electrolytes than that in liquid electrolytes. Improvement of J_{sc} due to the increase in I^- diffusion was also found in literature [33,39].

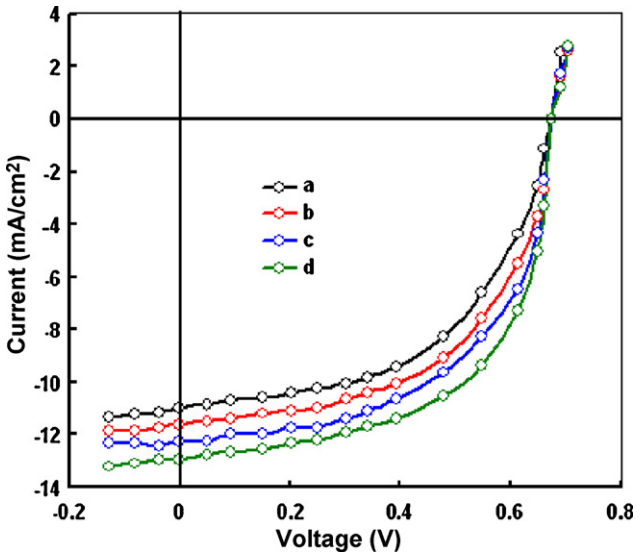

Fig. 10. Photovoltaic performance of DSSCs fabricated from **S** dye using polymer gel electrolytes with different PEO molecular weight. (a) 0.5×10^6, (b) 1.0×10^6, (c) 1.5×10^6 and (d) 2.0×10^6 under stimulated illumination intensity of 100 mW cm^{-2} at AM1.5.

4. Conclusions

Three new dyes **C1**, **C2** and **S**, based on 2-styryl-5-phenylazopyrrole, which contain one carboxy, two carboxy and one sulfonic acid anchoring groups, respectively were synthesized. The hexyl chain attached to the nitrogen of the central pyrrole ring enhanced the solubility of the dyes. The dyes showed long-wavelength absorption maximum around 620 nm and optical band gap of 1.66–1.68 eV. The quasi solid state DSSCs have been fabricated using these dyes as sensitizer and polymer gel electrolyte containing iodine /tri-iodide redox couple as redox mediator and characterized through their current–voltage characteristics and electrochemical impedance spectra (EIS). The overall PCE of the DSSCs are 4.17, 3.26 and 2.59% for **S**, **C2** and **C1**, respectively. The higher PCE for DSSCs with dye **S** as sensitizer has been attributed to the higher dye loading at TiO_2 surface, broad absorption spectra and longer electron lifetime. The lower PCE in the case of dye **C1** is ascribed to the reduction of the photocurrent and IPCE due to the lower dye loading on the TiO_2 surface. The PCE can be further improved by increasing the molecular weight of PEO in the polymer electrolyte. The overall PCE is about 4.8% for the DSSC sensitized with dye **S** based on polymer gel electrolyte consisting of PEO molecular weight of 2.0×10^6. This enhancement in PCE has been mainly attributed to the improvement in J_{sc} due to the increase in the diffusion coefficient of iodide ions in the electrolyte. It is likely that incorporation of appropriate number of the extra electron donor and acceptor groups in the dye structure will further improve the performance of the DSSCs based on these dyes. The longer electron life time can also be beneficial to improve the PCE of the cell, which can be achieved through the reduction of dye aggregation during the dye sensitization.

References

[1] (a) B. O.Regan, M. Grätzel, Nature 353 (1991) 737;
(b) A. Hagfeldt, M. Grätzel, Chem. Rev. 95 (1995) 49;
(c) M. Grätzel, Nature 414 (2001) 338.

[2] (a) M.K. Nazeeruddin, P. Pechy, T. Renouard, S.M. Zakeeruddin, R. Humphry-Baker, P. Comte, P. Liska, L. Cevey, E. Costa, V. Shklover, L. Spiccia, G.B. Deacon, C.A. Bignozzi, M. Grätzel, J. Am. Chem. Soc. 123 (2001) 1613;
(b) M.K. Nazeeruddin, F. De Angelis, S. Fantacci, A. Selloni, G. Viscardi, P. Liska, S. Ito, T. Bessho, M. Grätzel, J. Am. Chem. Soc. 127 (2005) 16835;
(c) M. Grätzel, J. Photochem. Photobiol. A 164 (2004) 3;
(d) C.Y. Chen, M. Wang, J.Y. Li, L. Alibabaei, C. Nogcle, J.D. Decoppet, J.H. Tsai, C. Gratzel, C.G. Wu, S.M. Zakeeruddin, M. Gratzel, ACS Nano 130 (2009) 3103.
[3] (a) S. Ito, S.M. Zakeeruddin, R. Humphry-Baker, P. Liska, R. Charvet, P. Comte, M.K. Nazeeruddin, P. Pechy, M. Takata, H. Miura, S. Uchida, M. Grätzel, Adv. Mater. 18 (2006) 1202;
(b) T. Horiuchi, H. Miura, K. Sumioka, S. Uchida, J. Am. Chem. Soc. 126 (2004) 12218;
(c) Z.S. Wang, F.Y. Li, C.H. Huang, J. Phys. Chem. B 105 (2001) 9210;
(d) K. Hara, T. Sato, R. Katoh, A. Furube, Y. Ohga, A. Shinpo, S. Suga, K. Sayama, H. Sugihara, H. Arakawa, J. Phys. Chem. B 107 (2003) 597.
[4] D. Hagberg, T. Edvinsson, T. Marinado, G. Boschloo, A. Hagfeldt, L. Sun, Chem. Commun. 21 (2006) 2245.
[5] S. Kim, J.K. Lee, S.O. Kang, J. Ko, J.H. Yum, S. Fantacci, F. De Angelis, D.D. Censo, M.K. Nazeeruddin, M. Grätzel, J. Am. Chem. Soc. 128 (2006) 16701.
[6] J.T. Lin, P.C. Chen, Y.S. Yen, Y.C. Hsu, H.H. Chou, M.C.P. Yeh, Org. Lett. 11 (2009) 97.
[7] Y.S. Yen, Y.C. Hsu, J.T. Lin, C.W. Chang, C.P. Hsu, D.J. Yin, J. Phys. Chem. C 112 (2008) 12557.
[8] (a) J. Nakazaki, I. Chung, M.M. Matsushita, T. Sugawara, R. Watanabe, A. Izuoka, Y. Kawada, J. Mater. Chem. 13 (2003) 1011;
(b) B.K. Banik, S. Samajdar, I. Banik, J. Org. Chem. 69 (2004) 213.
[9] C. Cannizzo, S. Amigoni-Gerbier, M. Frigoli, C. Larpent, J. Polym. Sci. Part A: Polym. Chem. 10 (2008) 3375.
[10] R. Fernández, I. Mondragon, P.A. Oyanguren, M.J. Galante, React. Funct. Polym. 1 (2008) 70.
[11] T. Carofiglio, C. Fregonese, G.J. Mohr, F. Rastrelli, U. Tonellato, Tetrahedron 7 (2006) 1502.
[12] L. Brigo, T. Carofiglio, C. Fregonese, F. Meneguzzi, G. Mistura, M. Natali, U. Tonellato, Sens. Actuators B: Chem. 1 (2008) 477.
[13] A. Vig, K. Sirbiladze, H.J. Nagy, P. Aranyosi, I. Rusznαk, P. Sallay, Dyes Pigments 71 (2006) 199.
[14] M.M.M. Raposo, A.M.R.C. Sousa, A.M.C. Fonseca, G. Kirsch, Tetrahedron 61 (2005) 8249.
[15] J.A. Mikroyannidis, M.S. Roy, G.D. Sharma, J. Power Sources 195 (2010) 5391.
[16] J.A. Mikroyannidis, A. Kabanakis, P. Balraju, G.D. Sharma, J. Phys. Chem. C 114 (2010) 12355.
[17] G.R. Robertson, Org. Synth. Coll. 1 (1941) 396;
G.R. Robertson, Org. Synth. Coll. 2 (1922) 57.
[18] A.D. Josey, E.L. Jenner, J. Org. Chem. 27 (1962) 2466.
[19] S. Zheng, A. Leclercq, J. Fu, L. Beverina, L.A. Padilha, E. Zojer, K. Schmidt, S. Barlow, J. Luo, S.-H. Jiang, A.K.-Y. Jen, Y. Yi, Z. Shuai, E.W. Van Stryland, D.J. Hagan, J.-L. Brédas, S.R. Marder, Chem. Mater. 19 (2007) 432.
[20] (a) L.M. Peter, N.W. Duffy, R.L. Wang, K.G.U. Wijayantha, J. Electroanal. Chem. 524 (2002) 127;
(b) N.W. Duffy, L.M. Peter, R.M.G. Rajapkse, K.G.U. Wijayabtha, Electrochem. Commun. 2 (2000) 658.
[21] L.J. Bellamy, The Infra-red Spectra of Complex Molecules, Chapman and Hall/John Wiley & Sons, London/New York, 1975, p. 304.
[22] (a) Q.J. Sun, H.Q. Wang, Y.H. Yang, Y.F. Li, J. Mater. Chem. 13 (2003) 800;
(b) Y. Li, Y. Cao, J. Gao, D. Wang, G. Yu, A.J. Heeger, Synth. Met. 99 (1999) 243.
[23] K. Hara, T. Sato, R. Katoh, A. Furube, T. Yoshihara, M. Murai, M. Kurashige, S. Ito, A. Shinpo, S. Suga, H. Arakawa, Adv. Funct. Mater. 15 (2005) 246.
[24] (a) G. Boschloo, A. Hagfeldt, J. Phys. Chem. B 109 (2005) 12093;
(b) P. Wang, S.H. Zakeeruddin, J.E. Moser, M. Grätzel, J. Phys. Chem. B 107 (2003) 13280.
[25] (a) M.A. Green, Solar Cells: Operating principles, Technology and system Applications, Prentice Hall, Englewood Cliffs, NJ, 1982;
(b) A. Usami, S. Seki, Y. Mita, H. Kobayashi, H. Miyashiro, N. Terada, Sol. Energy Mater. Sol. Cells 93 (2009) 840.
[26] (a) Z.S. Wang, G. Zhou, J. Phys. Chem. C 113 (2009) 15417;
(b) J.R. Jennings, Q. Wang, J. Phys. Chem. C 114 (2010) 1715.
[27] J. Rowley, G.J. Meyer, J. Phys. Chem. C 113 (2009) 447.
[28] Y. Liang, F. Cheng, J. Liang, J. Chen, J. Phys. Chem. C 114 (2010) 15842.
[29] Y. Ogomi, Y. Kashiwa, Y. Noma, Y. Fujita, S. Kojima, M. Moon, Y. Yamaguchi, S. Hayase, Sol. Energy Mater. Sol. Cells 93 (2009) 1009.
[30] C. Kanimozhi, P. Balraju, G.D. Sharma, S. Patil, J. Phys. Chem. C 114 (2010) 3287.
[31] (a) Q. Wang, J. Moser, M. Grätzel, J. Phys. Chem. B 109 (2005) 14945;
(b) Z. Wang, N. Koumura, Y. Cui, M. Takahashi, H. Sekiguchi, A. Mori, T. Kubo, A. Furube, K. Hara, Chem. Mater. 20 (2008) 3993;
(c) D. Kuang, S. Uchida, R. Humphry-Baker, S. Zakeeruddin, M. Grätzel, Angew. Chem. Int. Ed. 47 (2008) 1923;
(d) D. Zhao, T. Peng, L. Lu, P. Cai, P. Jiang, Z. Bian, J. Phys. Chem. C 112 (2008) 8486;
(e) M. Adachi, M. Sakamoto, J. Jiu, Y. Ogata, S. Isoda, J. Phys. Chem. B 110 (2006) 13872.
[32] F. Fabregat-Santiango, J. Bisquert, L. Cevey, P. Chen, M. Wang, S.M. Zakeeruddin, M. Grätzel, J. Am. Chem. Soc. 131 (2009) 558.
[33] K. Hara, K. Miyamoto, Y. Abe, M. Yanagida, J. Phys. Chem. B 109 (2005) 23776.
[34] Z. Lan, J.H. Wu, J.M. Lin, M. Huang, S. Lin, T. Sato, Electrochim. Acta 52 (2007) 6673.
[35] (a) J. Kang, W. Li, X. Wang, Y. Lin, X. Li, X. Xiano, S. Fang, J. Appl. Electrochem. 34 (2004) 301;
(b) Z. Lan, J.H. Wu, J.M. Lin, M. Huang, P. Li, Q. Li, Electrochim. Acta 53 (2008) 2296.
[36] J.B. Xia, F.Y. Li, C.H. Huang, J. Zhai, L. Jiang, Sol. Energy Mater. Sol. Cells 90 (2006) 944.
[37] J.H. Wu, Z. Lan, J.M. Lin, M. Huang, S. Hao, L. Feng, Electrochim. Acta 52 (2007) 7128.
[38] T. Miyamoto, K. Shibayama, J. Appl. Phys. 44 (1973) 5372.
[39] J.G. Chen, C.Y. Chen, S.J. Wu, J.Y. Li, C.G. Wu, K.C. Ho, Sol. Energy Mater. Sol. Cells 92 (2008) 1723.